Contents lists available at ScienceDirect

BBA - General Subjects

journal homepage: www.elsevier.com

# Novel insights into the transport mechanism of the human amino acid transporter LAT1 (SLC7A5). Probing critical residues for substrate translocation

Lara Napolitano [a], Michele Galluccio [a], Mariafrancesca Scalise [a], Chiara Parravicini [b], Luca Palazzolo [c], Ivano Eberini [b], Cesare Indiveri [a, *]

[a] Department DiBEST (Biologia, Ecologia, Scienze della Terra) Unit of Biochemistry and Molecular Biotechnology, University of Calabria, Via P. Bucci 4C, 87036 Arcavacata di Rende, Italy
[b] Dipartimento di Scienze Farmacologiche e Biomolecolari, Università degli Studi di Milano, Italy
[c] Dipartimento di Scienze Farmacologiche e Biomolecolari e Dipartimento di Scienze Biomediche e Cliniche "L. Sacco", Università degli Studi di Milano, Italy

ARTICLE INFO

*Article history:*
Received 28 September 2016
Received in revised form 21 December 2016
Accepted 10 January 2017
Available online xxx

*Keywords:*
Liposome
Membrane transporter reconstitution
Docking
Recombinant protein expression
Site-directed mutagenesis

ABSTRACT

*Background*
LAT1 (SLC7A5) is the transport competent unit of the heterodimer formed with the glycoprotein CD98 (SLC3A2). It catalyzes antiport of His and some neutral amino acids such as Ile, Leu, Val, Cys, Met, Gln and Phe thus being involved in amino acid metabolism. Interestingly, LAT1 is over-expressed in many human cancers that are characterized by increased demand of amino acids. Therefore LAT1 was recently acknowledged as a novel target for cancer therapy. However, knowledge on molecular mechanism of LAT1 transport is still scarce.
*Methods*
Combined approaches of bioinformatics, site-directed mutagenesis, chemical modification, and transport assay in proteoliposomes, have been adopted to unravel dark sides of human LAT1 structure/function relationships.
*Results*
It has been demonstrated that residues F252, S342, C335 are crucial for substrate recognition and C407 plays a minor role. C335 and C407 cannot be targeted by SH reagents. The transporter has a preferential dimeric structure and catalyzes an antiport reaction which follows a simultaneous random mechanism.
*Conclusions*
Critical residues of the substrate binding site of LAT1 have been probed. This site is not freely accessible by molecules other than substrate. Similarly to LeuT, $K^+$ has some regulatory properties on LAT1.
*General significance*
The collected data represent a solid basis for deciphering molecular mechanism underlying LAT1 function.



## 1. Introduction

LAT1 (SLC7A5) is a $Na^+$ and pH-independent amino acid antiporter with 12 predicted transmembrane α-helices (TMs) (Uniprot ID: Q01650) that regulates distribution of specific amino acids across cell membranes. It was described as a branched chain amino acid transporter [1] and, more recently, it was shown that His is one of the major substrate [2]. LAT1 belongs to a special group of Heterodimeric Amino acid Transporters (HATs) structurally coupled to the glycoprotein CD98 (SLC3A2). The interaction occurs through a conserved disulfide between C164 of hLAT1 and C109 of hCD98 [1]. The interest on this peculiar transporter increased a lot in the recent years since its over-expression in many tumors has been described; therefore, LAT1 is now considered a novel pharmacological target [3,4].

However, identification or design of potent inhibitors to be proposed as potential drugs, requires a deep knowledge of the target structure and action mechanism that, in the case of LAT1, are still missing. Indeed, besides the well-known functional properties of the heterodimeric complex LAT1/CD98, information on structure/function relationships are only predicted by in silico methodologies [5].

The tissue distribution of LAT1 is quite narrow but it becomes wider in tumors [6–9]. Canonical sub-cellular localization for LAT1 is the plasma membrane where it catalyzes inwardly directed flux of His, Ile, Leu, Val, Cys, Met, Gln and some other neutral amino acids, in antiport with His, Tyr or Gln; LAT1 activity is combined to the action of other amino acid transporters whose expression is often redundant [3,10].

Due to its capacity of exchanging Gln with other amino acids, LAT1 is involved in "Glutamine addiction", a typical hallmarks of tumors. In fact, this transporter, together with its companion ASCT2 (SLC1A5) gives rise to a combined transport cycle of Gln and Leu, used for both cancer growth and progression [11]. Indeed it is considered a prognostic marker of malignancy [6–9]. Very recently, a role

**Abbreviations:** DTE, dithioerythritol; BCH, 2-amino-2-norbornanecarboxylic acid; $C_{12}E_8$, octaethylene glycol monododecyl ether; MTSEA, 2-Aminoethyl methanethiosulfonate hydrobromide; NEM, N-ethylmaleimide

* Corresponding author.
Email address: cesare.indiveri@unical.it (C. Indiveri)

http://dx.doi.org/10.1016/j.bbagen.2017.01.013
0304-4165/

of LAT1 in cell signaling has been proposed due to an alternative localization in the lysosomal membrane [12] where it transports Leu, thus transducing amino acids sufficiency to mTORC1 together with SLC38A9 which transports Gln and Arg [13,14].

The role of CD98 in the heterodimer formation/activity has been matter of investigation for years. Only recently, it has been demonstrated that LAT1 is the sole transport competent unit while CD98 does not play any role in the intrinsic transport function [2]. This correlates well with the finding that CD98 is a multifunctional protein with other functions unrelated to transport, such as integrin signaling [15] or oxidative stress response [16]. The hypothesis is that CD98 may function mainly as molecular chaperone routing LAT1 [17] or other transporters to its definitive localization in plasma (or intracellular) membrane.

In some elegant studies the homology structural model of hLAT1 has been built using, as template, the bacterial AdiC transporter, whose structure has been solved by X-ray crystallography and hypothetical LAT1 inhibitors have been used for docking analysis [5,18–21]. In the present work, the homology model of LAT1 was constructed allowing us to predict amino acid residues critical for substrate recognition and translocation. Interestingly, some of these residues correspond to those previously suggested [18] and a novel one was identified. For the first time, the role of these residues has been demonstrated by combined approaches of site-directed mutagenesis, chemical modification, and transport assay in proteoliposomes. This novel information on LAT1 structure/function relationships may have also important outcomes in cancer drug design.

## 2. Materials and methods

### 2.1. Materials

His Trap HP columns, PD-10 columns, ECL plus and Hybond ECL membranes were purchased from GE Healthcare; anti-hLAT1 and anti-rabbit IgG HRP conjugate from Cell Signalling (5347S Lot1 and 7074S Lot 25 respectively); anti-His HRP conjugate from Sigma-Aldrich (A7058); radiolabeled amino acids were purchased from ARC (American Radiolabeled Chemicals); all the other reagents are from Sigma-Aldrich.

### 2.2. Construction and over-expression of recombinant hLAT1 proteins

The mutagenesis of hLAT1 has been performed by PCR overlap extension method as described in [22,23] by using primers reported in Table 1. hLAT1 WT and mutant proteins have been over-expressed in *E. coli* Rosetta(DE3)pLysS as described in [24].

**Table 1**
Sequences of primers used for mutagenesis. The modified codons are in underlined italic.

| | |
|---|---|
| LAT1 F252A forward | ATTATACAGCGGCCTC*GCG*GCCTATGGAGGATG |
| LAT1 F252A reverse | CATCCTCCATAGGC*CGC*GAGGCCGCTGTATAAT |
| LAT1 F252W forward | ATTATACAGCGGCCTC*TGG*GCCTATGGAGGATG |
| LAT1 F252W reverse | CATCCTCCATAGGC*CCA*GAGGCCGCTGTATAAT |
| LAT1 C335A forward | TTCGTGGGCCTGTCC*GCC*TTCGGCTCCGTCAAT |
| LAT1 C335A reverse | ATTGACGGAGCCGAA*GGC*GGACAGGCCCACGAA |
| LAT1 S342G forward | CGGCTCCGTCAATGGG*GGC*CTGTTCACATCCTCC |
| LAT1 S342G reverse | AGGATGTGAACAG*GCC*CCCATTGACGGAGC |
| LAT1 C407A forward | TTCTTCAACTGGCTC*GCC*GTGGCCCTGGCCATC |
| LAT1 C407A reverse | GATGGCCAGGGCCAC*GGC*GAGCCAGTTGAAGAA |

### 2.3. Purification of hLAT1

hLAT1, over-expressed in *E. coli*, has been purified as previously described with some modifications [24]. In brief, cell lysates were solubilized, centrifuged (12,000*g*, 10 min, 4 °C) and the purification has been performed using ÄKTA start. The supernatant was applied on a His Trap HP column (5 mL Ni-Sepharose) equilibrated with 10 mL buffer (20 mM Tris HCl pH 8.0, 10% glycerol, 200 mM NaCl, 0.1% sarkosyl, and DTE 2 mM). 10 mL of buffer (20 mM Tris HCl pH 8, 10% glycerol, 200 mM NaCl, 0.05% n-Dodecyl β-D-maltoside and 2 mM DTE) was used to wash column while the protein was eluted with the same buffer plus 400 mM imidazole. Imidazole was removed using a PD-10 column by desalting 2.5 mL of the purified protein collected in 3.5 mL of desalt buffer (20 mM Tris HCl pH 8, 10% glycerol, 0.05% n-Dodecyl β-D-maltoside and 10 mM DTE).

### 2.4. Reconstitution of the purified hLAT1

The desalted hLAT1 was reconstituted by removing detergent from mixed micelles of detergent, protein and phospholipids using batch wise method as previously described [2] with the modification of the time of incubation with 0.5 g Amberlite XAD-4 performed at room temperature for 90 min. The initial mixture contained: 4 μg of purified protein, 100 μL of 10% $C_{12}E_8$, 100 μL of 10% egg yolk phospholipids (w/v) in the form of liposomes prepared as previously described [25], 20 mM Tris HCl pH 7.5 and 10 mM L-His, except were differently indicated, in a final volume of 700 μL.

### 2.5. Transport measurements

Uptake experiments were performed by removing the external substrate through the flow of 600 μL of proteoliposomes on a Sephadex G-75 column (0.7 cm diameter × 15 cm height) pre-equilibrated with 20 mM Tris HCl pH 7.5 and sucrose at an appropriate concentration to balance internal osmolarity. Transport was started by adding 5 μM [$^3$H]His to proteoliposomes containing 10 mM His, except were differently indicated. Transport was stopped by a mixture of 100 μM BCH and 1.5 μM $HgCl_2$ at the indicated times; for the controls samples the mixture of inhibitors was added at time zero according to the inhibitor stop method [26]. At the end of the transport assay, 100 μL proteoliposomes was passed through a Sephadex G-75 column (0.6 cm diameter × 8 cm height), to separate the external from the internal radioactivity. Liposomes were eluted with 1 mL 50 mM NaCl in 4 mL scintillation mixture and counted. Experimental values were obtained by subtracting controls: for the measurement of initial transport rate, the reaction was stopped after 15 min, i.e., within the initial linear range of [$^3$H]His uptake in proteoliposomes, except where differently indicated. To calculate transport rate, IC50 values or kinetic parameters, Grafit 5.0.13 software has been used for fitting data in first order rate, dose response or Michaelis–Menten and Lineweaver-Burk equations, respectively. Km values similar to the WT or to previous literature data, are reported in the Results section with S.D. but not shown graphs. All these data derive from three experiments. Protein concentration was estimated by Chemidoc imaging system to calculate the hLAT1 specific activity [27].

### 2.6. Ultracentrifugation of proteoliposomes

500 μL of samples were ultracentrifuged (110,000*g*, 1 h 30 min, 4 °C) after passage through Sephadex G-75 column to separate hLAT1 reconstituted proteoliposomes from liposomes without incorporated proteins as previously described [2]. The obtained pellet was solubilized with 3% sarkosyl for western blot analysis.

### 2.7. Western blot analysis

Western blot analysis were performed using anti-LAT1 antibody 1:2000 or anti-His antiserum 1:1000 to immuno-detect hLAT1. The reaction has been performed over night at 4 °C for anti-LAT1 antibody and detected by Electro Chemi Luminescence (ECL) assay after an incubation of 1 h with secondary antibody anti-rabbit 1:5000. For anti-His HRP conjugate the reaction has been performed for 1 h at room temperature and detect by Electro Chemi Luminescence (ECL) at the end of incubation.

### 2.8. Comparative modelling and quality validation

A multiple alignment of some members of the amino acid-polyamine-organocation (APC) superfamily was carried out through the multiple alignment program ClustalW, including 3 amino acid/polyamine antiporters (APC), AdiC, CadB and PotE, 1 cationic amino acid transporter (CAT), CAT6, 1 amino acid/choline transporter (ACT), Uga4, 1 glutamate/GABA antiporter (GGA), GadC, the large neutral amino acid transporters LAT2, and our target protein hLAT1. This multiple alignment has been used to carry out the comparative modelling of hLAT1 via the Molecular Operating Environment (MOE) Homology Model software with default settings. Three different models for hLAT1 were generated: an outward open holo monomeric form, 3OB6 [28]; an outward closed holo monomeric form, 3L1L [20]; and outward open apo dimeric form, 3LRB [29]. All the refinement procedures were based on molecular mechanics with the Amber12:EHT force field. The PSIPRED Protein Sequence Analysis Workbench (http://bioinf.cs.ucl.ac.uk/psipred/) and the TMHMM Server (http://www.cbs.dtu.dk/services/TMHMM/) were also used to predict LAT1 secondary structure and the TM helices. In order to operate a quality validation, a solvent/membrane explicit molecular dynamics (MD) simulation was carried out on the outward-closed monomeric holo form of hLAT1 by GROMACS [30]. As a first step, Desmond, a Schrodinger tool [31], was used to insert hLAT1 into a pre-equilibrated model of membrane bilayer composed by 212 POPC. hLAT1 was oriented into the membrane model keeping the longest axis of the protein perpendicular to the membrane surface. The system was solvated with 15538 TIP3P water molecules.

Then, the system was equilibrated for 100 ps at 300 K, applying pressures independently in the *x*, *y*, and *z* directions using the Berendsen coupling method [32], and 1000 ps of NPT equilibration at 1.0 Bar using Nose-Hoover thermostat [33]. At last, a 50 ns MD simulation was carried out with the following parameters: 300 K, 1 bar, Nose-Hoover temperature and Parrinello-Rahman pressure couplings, 2 fs of integration time step. The N- and C-terminal domains were capped and the Charmm36 force field was used in all MD steps.

### 2.9. Identification of hLAT1 binding site

hLAT1 binding site was identified through the MOE Site Finder module, which uses a geometric approach to calculate possible binding sites in a receptor starting from its 3D atomic coordinates. This method is based not on energy models but on alpha spheres, which are a generalization of convex hulls [34].

### 2.10. Molecular docking of His in the hLAT1 binding site

His was docked always in zwitterionic form with respect to the Cα-bound carboxylic and aminic groups. The Nδ and Nε tautomers and the protonated form of the imidazole heteroaromatic ring were generated and tested.

Molecular docking was carried out through the MOE Docking program with default settings and the Amber12:EHT force field, using both the monomeric hLAT1 models as receptors and the dummy atoms created by Site Finder as explored site. The receptor was considered as a rigid body.

### 2.11. Protein mutation design

C335A and C407A mutations were introduced in the hLAT1 models through the MOE Protein Design program, and the variation of His affinity (Δ affinity) of mutant hLAT1 was computed with respect to the wild-type. Also the Protein Design program was run with the Amber12:EHT force field.

## 3. Results

### 3.1. Identification of crucial amino acid residues

The structural model of hLAT1 was built by homology, using as template the bacterial AdiC, whose crystallographic structure is currently available in different conformational states within the transport cycle: the open-to-out apo form (PDB ID 3LRB and 3NCY) [29,35], the substrate-bound open-to-out form (PDB ID 3OB6) [28], and the outward-facing $Arg^+$-bound occluded (PDB ID 3L1L) conformation [20]. In line with already published alignments, due to the low sequence identity shared between hLAT1 and AdiC, also other members of APC transporter family, were included in the alignment, among which the large neutral amino acids transporter 2 (LAT2), the glutamate:gamma-aminobutyrate antiporter (GadC), the lysine:cadaverine antiporter (CadB), the ornithine:putrescine antiporter (PotE), the GABA-specific permease (Uga4), and the cationic amino acid transporter 6 (Cat6) [18,29] (Fig. 1). Helices of LAT1 are highlighted in Supplemental Fig. 1 as derived from hydropathy plot of Supplemental Fig. 2 [36]. Notably, the last published structure of AdiC [21] revealed the same characteristics of that built in this work (not shown, but see Supplemental Fig. 3). In analogy to AdiC, hLAT1 could form a homodimer (Fig. 2A) in which monomers are present either in outward-open (Fig. 2B) or closed (Fig. 2C) forms. To predict some of the crucial residues for substrate binding and transport, the alignment with AdiC was considered (Fig. 1 and Supplemental Fig. 1). The residues of AdiC W202, W293 and S357 which are important for substrate (agmatine/Arg) binding and translocation [20,21,28] corresponded to LAT1 F252, S342 and, C407, respectively (Fig. 1) as also reported in Geier et al. [18]. The structural stability and the quality of the hLAT1 homology model were confirmed by the analysis of the molecular dynamics trajectory. The root means square deviation (RMSD) for the main chain shows that the protein reaches a plateau at 0.27 nm after approx. 20 ns (Supplemental Fig. 4). A low RMSD value (0.21 nm) was also obtained when the starting protein structure and the final MD frame (Supplemental Fig. 5) were superposed. A z-section of the whole simulated system (hLAT1, membrane and solvent) is depicted in Supplemental Fig. 6.

Docking simulations on LAT1 outward open form highlighted an additional Cys residue, besides C407, never predicted before and close to the substrate binding site F252, i.e., C335 (Fig. 3A). Docking simulations performed on the outward closed conformation show that all the poses, obtained for the natural LAT1 substrate His, well fit with the position of the Arg substrate in AdiC, and that the residues surrounding the binding site include F252, S342 and C407 (Fig. 3 B) [20]. A comparison between the hLAT1 and the AdiC binding sites is shown in Supplemental Fig. 3. As reported in Geier et al. [18], our model confirmed that the hLAT1 binding site volume is greater than the AdiC one, and this is due to the substitutions of the corresponding residues between the two primary structures, e.g. W202 is replaced

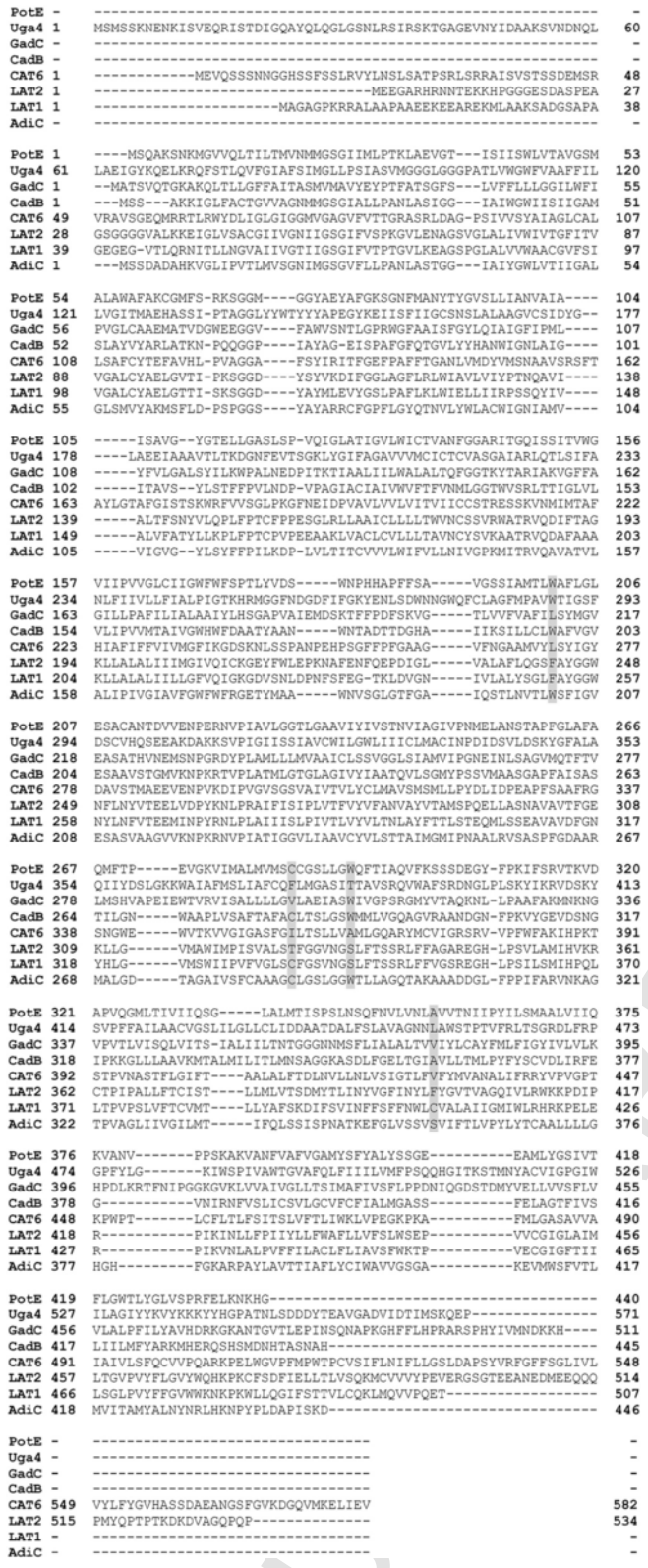

**Fig. 1.** Critical amino acids discovery. Complete alignment of hLAT1 with orthologous members of the APC transporter family has been performed as described in Section 2.8. The crucial amino acids identified and then mutated are shadowed in grey. AdiC: Arginine/agmatine antiporter (P60061); PotE: ornithine/putrescine antiporter (P0AAF1); Uga4: GABA-specific permease (P32837); GadC: glutamate/gamma-aminobutyrate antiporter (P63235); CadB lysine/cadaverine antiporter (P0AAE8); Cat6: cationic amino acid transporter 6 (Q9LZ20); LAT2: large neutral amino acids transporter 2 (Q9UHI5); LAT1: large neutral amino acids transporter 1 (Q01650).

by F252 and W293 by S342 (Fig. 1). To investigate the actual role of these residues, mutants were constructed and the corresponding recombinant proteins were produced in *E. coli* and purified as described in Sections 2.2 and 2.3. F252 was substituted either by a conservative residue, corresponding to the AdiC homologue (F252W), or by a non-conservative residue (F252A), changing the chemical/steric properties of the side chain. The transport activity of the mutant proteins was tested in proteoliposomes as $His_{ex}/His_{in}$ antiport (Fig. 4A) to evaluate possible loss of function. Interestingly, the substitution F252A completely abolished transport activity; while, substitution F252W only impaired transport with respect to the WT. To gain further insights into this aspect, kinetic analysis was conducted on F252W. The measured Km (Fig. 4B) was 184 ± 40 μM, higher than that of WT [2]. The internal Km of F252W was very similar to that of WT, i.e., 2.0 ± 0.45 mM (Supplemental Fig. 7). The mutant S342G was also tested for activity (Fig. 4A). This protein was functional and the transport activity was similar to that of WT. The Km for His of S342G was much higher than that of WT with a value of 784 ± 139 μM (Fig. 4C); while the internal Km, i.e., 3.2 ± 0.49 mM (Supplemental Fig. 7), was similar to the WT Km. Cys mutants were generated substituting C335 or C407 or both with Ala. The time course of the two mutants showed that they are functional, even though C335A and the double mutant were less active than the WT (Fig. 5A). Km for substrate were measured on both the external and internal membrane sides. As shown in Fig. 5B, substitution of C335 strongly increased the external Km which was 582 ± 234 μM indicating that also C335 is crucial for substrate binding. C407A mutant showed a Km (37 ± 11 μM, Supplemental Fig. 8) similar to that of WT [2]. In silico mutants strongly confirmed this experimental evidence: the mutation of C335 to A reduces the affinity for the substrate to 2.4 kcal/mol, on the contrary, the same mutation on C407 does not modify the affinity for His with respect to the WT hLAT1 (0.1 kcal/mol). Internal Km was not influenced by the substitution of C335 (2.5 ± 0.67 mM) but slightly impaired by the substitution of C407, with a value of 5.9 ± 1.4 mM (Fig. 5C). The external Km of the double mutant was strongly impaired as in the case of C335A (775 ± 127 μM, Supplemental Fig. 9) while the internal one was similar to that of C407A (not shown).

### *3.2. Inhibition by mercury compounds*

To further investigate the topological relationships of the two Cys residues namely C335 and C407, the reactivity of WT and mutants towards SH reagents was tested. Indeed, it has been previously demonstrated that LAT1 interacts with mercury compounds [37,38]. Dose-response experiments for $HgCl_2$ were performed on WT, C335A, C407A and C335/407A (Fig. 6A). Very similar patterns were observed for WT and the mutants with comparable IC50 values: 0.90 ± 0.14 μM, 1.3 ± 0.13 μM, 1.3 ± 0.10 μM or 1.7 ± 0.12 μM for WT, C335A, C407A or C335/407A, respectively. These data ruled out the possible involvement of these Cys residues in the interaction with the mercury compound. The kinetic of inhibition of His transport by $HgCl_2$ (Fig. 6B) showed a non-competitive pattern demonstrating that the interaction of the mercury compound occurs via residues far from the substrate binding site. Other hydrophilic or hydrophobic SH reagents were also tested. Methyl-Hg, Ethyl-Hg, MTSEA and NEM inhibited approximately at the same extent the WT and the Cys mutants (Fig. 6C) confirming that the two Cys residues are not involved in interaction with SH reagents. The inhibition by mercury compounds was reversed by the S-S reducing agent DTE

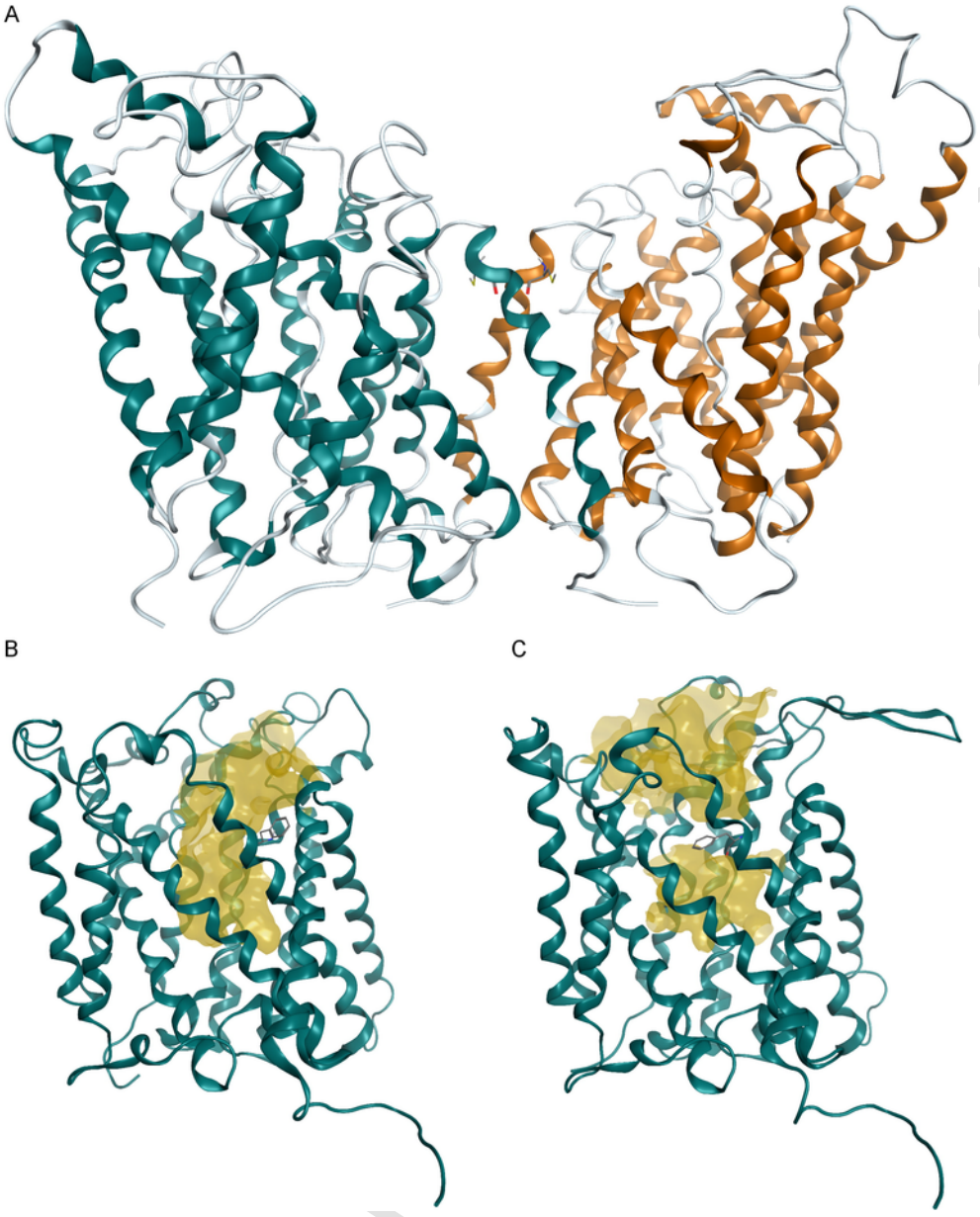


**Fig. 2.** hLAT1 homology models. hLAT1 is shown as ribbon representation in its dimeric, outward-open and outward-closed conformation in A), B) and C), respectively. Cys (C458) at the interface of LAT1 dimer are shown in stick representation in A). Similarly to residue W202 of AdiC, also the conserved residue F252 (stick representation), behaves like a gate in LAT1, hindering the substrate access pathway (yellow surface), as shown in B) and C).

(experiments not shown), proving the involvement of thiol group(s) of Cys residue(s) other than C335 or C407, in the inhibition.

### *3.3. Effect of intracellular cations on LAT1 transport activity*

As previously shown, His transport mediated by hLAT1 is not dependent on external $Na^+$ in agreement with data from intact cells [1]. By means of the proteoliposome model, the possible influence by intraliposomal (intracellular) ions on transport was investigated. Fig. 7A shows that internal $K^+$ stimulated His antiport with respect to the control, containing sucrose. K-gluconate and KCl exerted similar effects demonstrating that the $Cl^-$ was not involved in stimulation. $Na^+$ had a similar effect of that of $K^+$. Fig. 7B shows the dependence of stimulation on $K^+$ concentration. The activity increased along with the internal $K^+$ level reaching a plateau at 80 mM, i.e., a concentration not far from the physiological level. To understand if intraliposomal (intracellular) $K^+$ could affect transporter affinity towards its substrates, kinetic analysis was performed showing an increase of Vmax from 2.1 ± 0.16 to 3.1 ± 0.28 nmol $mg^{-1}$ $min^{-1}$, while the Km was not significantly influenced being 36.4 ± 6.7 μM or 36.0 ± 8.0 μM in absence or presence of internal $K^+$, respectively (Fig. 7C).

### *3.4. Kinetics and transport mechanism of LAT1*

The kinetic mechanism of the $His_{ex}/His_{in}$ antiport was investigated by a bi-reactant analysis. In this type of experiment, the concentrations of both external and internal substrates were varied in a single experiment [39,40]. The rate of [$^3$H]His uptake was plotted as function of the external (Fig. 8 A) or internal His (Fig. 8B) concentrations. Data were plotted according to Lineweaver-Burk, which allows

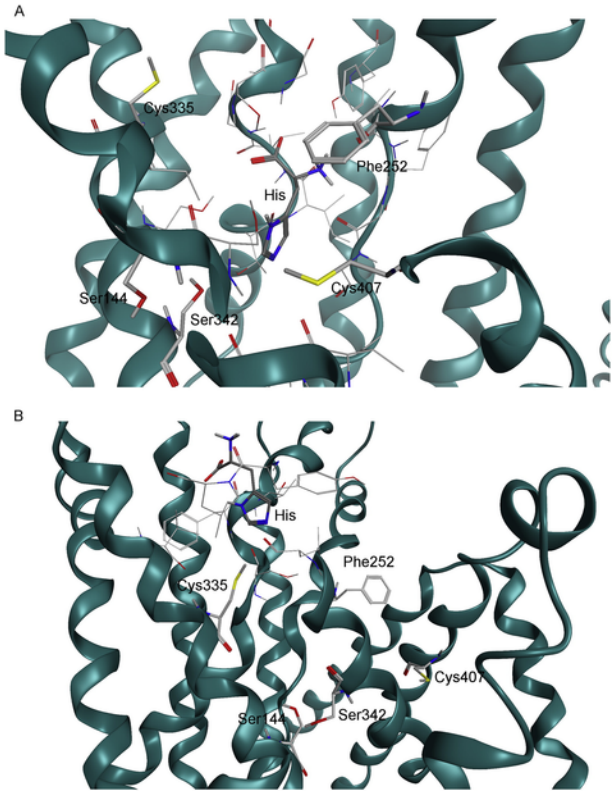


**Fig. 3.** hLAT1 Substrate binding site. Representative docking poses for His in LAT1 outward-open form A) and outward-closed form B). hLAT1 is shown in ribbon representation; His and residues of the binding site are shown as stick representation.

discriminating between ping-pong and simultaneous mechanisms [41]. In all the analysed reactions, the straight lines showed non parallel patterns intersecting in proximity of the X-axis. These data demonstrated that the $His_{ex}/His_{in}$ transport reaction follows a simultaneous mechanism that can be random or ordered. The first is characterized by no preferential binding order of the two substrates to the transporter; while in the ordered type, one of the two substrates binds first to the transporter. The two types can be discriminated by analyzing the dissociation constant of the ternary ($His_{ex}$-transporter-$His_{in}$) and binary transporter-His complexes [41,42]. These constants were calculated by re-plotting the values of the intercepts on the Y-axis or the slopes of the straight lines, as function of the reciprocal substrate concentrations (insets of Fig 8A and B). Concentration independent (Ks) values were 47.5 μM for external His and 5.6 mM for internal His. The $Ki_S$ values were 73 μM for external His and 9.5 mM for internal His, i.e., similar to the respective Ks values and fulfilling the relation $Ki_{S1} \cdot K_{S2} = Ki_{S2} \cdot K_{S1}$ which is typical of a random simultaneous mechanism. This implies that the two substrates bind at the same time to the external and internal sites. External Km for other substrates of LAT1, namely Leu, Met, Val, Gln or Ala was 25 ± 13 μM, 31 ± 11 μM, 57 ± 20 μM, 0.7 ± 0.4 mM or > 1 mM, respectively (experiments not shown). These values are in the same order of magnitude of those previously measured in intact cells, i.e., 19.7 μM, 20.2 μM, 47.2 μM, 1.6 mM for Leu, Met, Val, Gln, respectively. While no values of Km for Ala are available in intact cells [2,43,44]. This confirms that the functional properties of the recombinant protein resemble those of the native one.

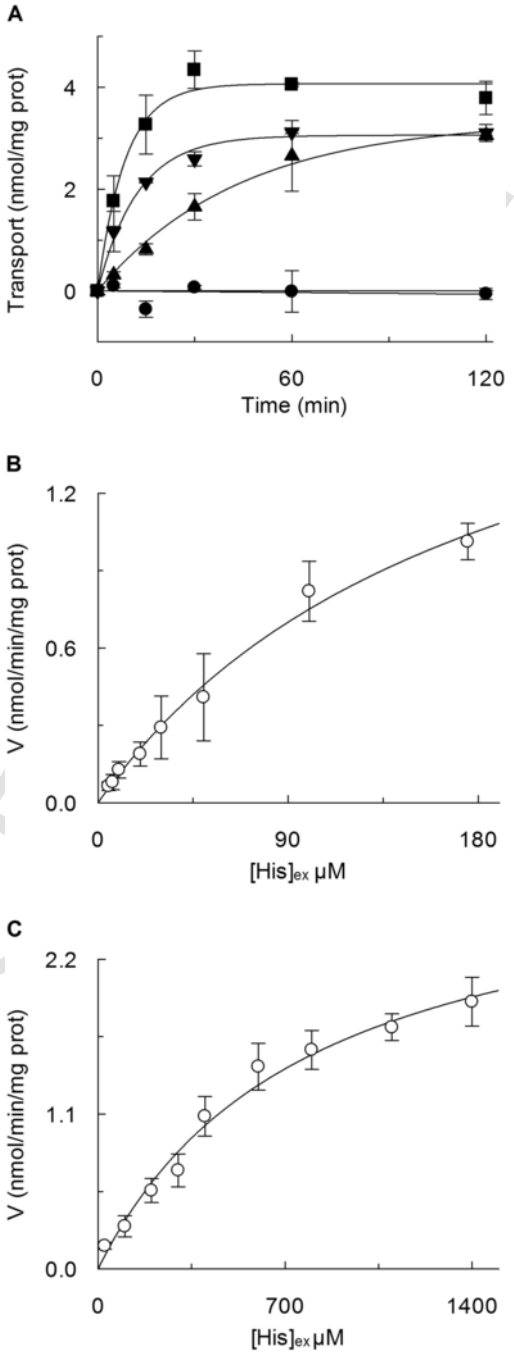


**Fig. 4.** [$^3$H]His uptake in proteoliposomes reconstituted with over-expressed hLAT1 WT and mutants. A) Transport was started adding 5 μM [$^3$H]His to proteoliposomes reconstituted with LAT1 WT (■), F252W (▲), F252A (●) or S342G (▼). Proteoliposomes contained 10 mM His and transport reaction was stopped at indicated times as described in Section 2.5. Data are plotted according to first rate equation. Results are mean ± S.D. from three independent experiments. B–C) Dependence of the rate of His antiport. The transport rate at 30 min was measured adding [$^3$H]His at the indicated concentration to proteoliposomes reconstituted with LAT1 F252W (B) or LAT1 S342G (C) containing 10 mM internal His. Data were plotted according to Michaelis–Menten equation. Results are mean ± S.D. from five independent experiments.

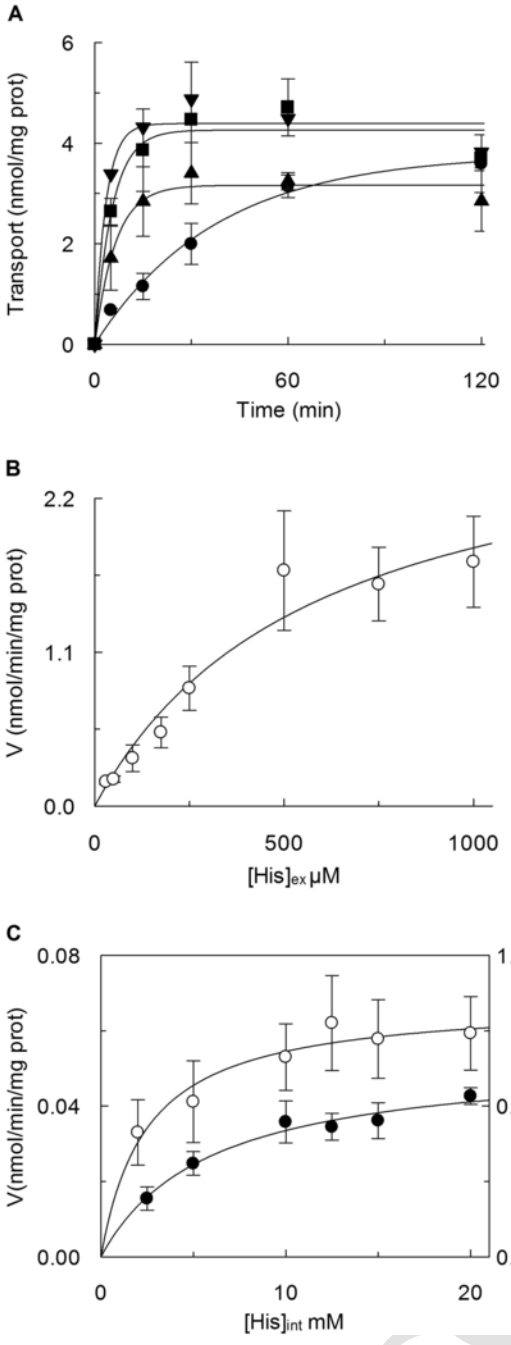


**Fig. 5.** [$^3$H]His uptake in proteoliposomes reconstituted with over-expressed hLAT1 WT and mutants. A) Transport was started adding 5 µM [$^3$H]His to proteoliposomes reconstituted with LAT1 WT (■), C335A (●), C407A (▼) or double mutant C335A/C407A (▲). Proteoliposomes contained 10 mM His and transport reaction was stopped at indicated times as described in Section 2.5. Data are plotted according to first rate equation. Results are mean ± S.D. from three independent experiments. B) Dependence of the rate of His antiport. The transport rate at 30 min was measured adding [$^3$H]His at the indicated concentration to proteoliposomes reconstituted with LAT1 C335A containing 10 mM internal His. Data were plotted according to Michaelis–Menten equation. Results are mean ± S.D. from three independent experiments. C) Dependence of the rate of His antiport. The transport rate at 30 min for C335A mutant and at 15 min for C407A mutant was measured adding 5 µM [$^3$H]His to proteoliposomes reconstituted with LAT1 C335A (○) or C407 (●) containing indicated concentrations of internal His. Data were plotted according to Michaelis-Menten equation, left y-axys corresponds to C335A data and right y-axis to C407A. Results are mean ± S.D. from three independent experiments.

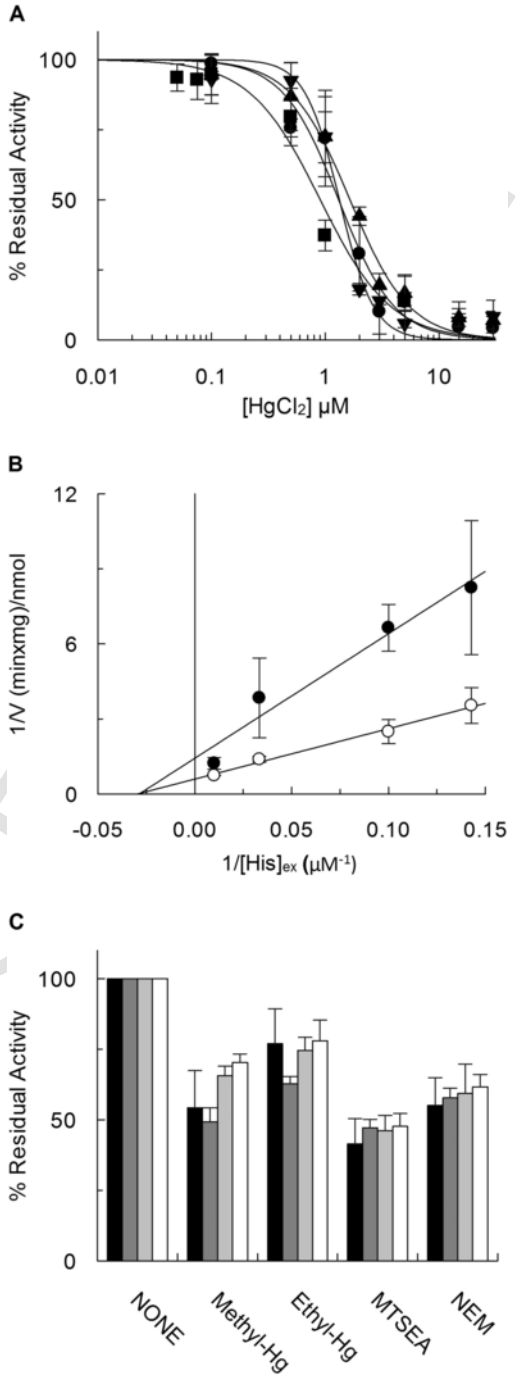


**Fig. 6.** Inhibition by SH-reagents of the recombinant hLAT1 in proteoliposomes. A) Dose-response curves for the inhibition by $HgCl_2$ of the hLAT1 WT and mutants. Transport was measured adding 5 µM [$^3$H]His to proteoliposomes containing 10 mM His reconstituted with LAT1 WT (■), C335A (●), C407A (▼) or double mutant C335A/C407A (▲) in the presence of indicated concentrations of $HgCl_2$. Transport was measured in 30 min as described in Section 2.5. Percent residual activity with respect to the control (without additions) is reported. Results are mean ± S.D. from three independent experiments. B) Kinetic analysis of the inhibition according to Lineweaver–Burk as reciprocal transport rate vs reciprocal His concentration; transport rate was measured adding 5 µM [$^3$H]His at the indicated concentrations to proteoliposomes containing 10 mM His and stopping the reaction after 15 min as described in Section 2.5. In (●) 0.8 µM $HgCl_2$ was added as inhibitor in comparison to samples without inhibitor (○). Results are mean ± S.D. from three independent experiments. C) Effect of Methyl-Hg, Ethyl-Hg, MTSEA and NEM on the LAT1 WT and Cys-mutants. Transport was measured adding 5 µM [$^3$H]His to proteoliposomes

containing 10 mM His reconstituted with LAT1 WT (black bar), C335A (dark gray bar), C407A (light gray bar) or C335A/C407A (white bar) in the presence of 5 μM Methyl-Hg, 12 μM Ethyl-Hg, 50 μM MTSEA or 500 μM NEM. Transport was measured in 30 min as described in Section 2.5. Percent residual activity with respect to the control (without additions) is reported. Results are mean ± S.D. from three independent experiments. Student's two tailed unpaired *t*-test was performed on the sample without external compounds (control) and no difference respect control have been observed within the $p$ value < 0.05. (For interpretation of the references to color in this figure legend, the reader is referred to the web version of this article.)

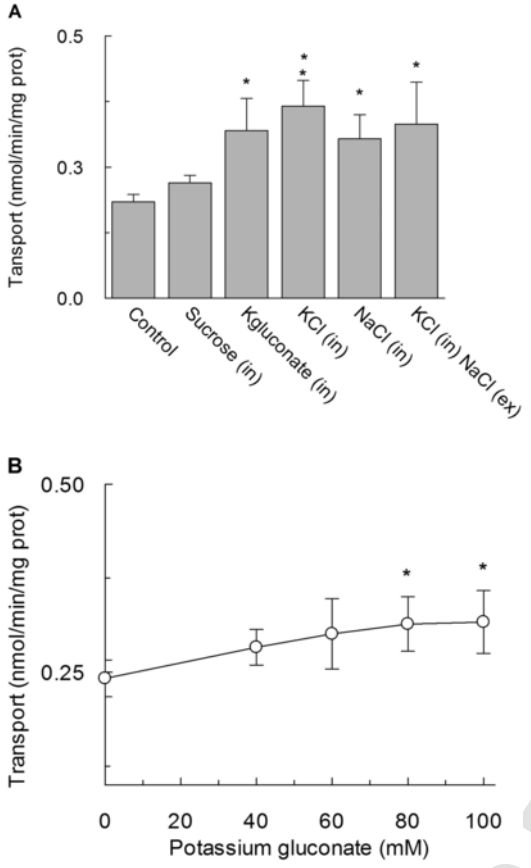


**Fig. 7.** Effects of intraliposomal salts on $His_{ex}/His_{in}$ transport in proteliposomes. A) The reconstitution was performed as described in Section 2.4. Transport was started adding 5 μM [$^3$H]His to proteoliposomes containing 10 mM His and 100 mM of indicated salts. Sucrose at 200 mM was used as control of osmotic stress. Effect of 100 mM NaCl added to the extraliposomal compartment was also evaluated. Transport reaction was stopped at 30 min as described in Section 2.5. Results are mean ± S.D. from three independent experiments. B) Transport was started adding 5 μM [$^3$H]His to proteoliposomes containing 10 mM His and indicated concentration of Potassium gluconate and stopped at 30 min as described in Section 2.5. Results are mean ± S.D. from three independent experiments. Student's two tailed unpaired *t*-test was performed on the sample without internal compounds (control); $p$ values were symbolized as follows: $^*p < 0.05$; $^{**}p < 0.01$ (A–B). C) Dependence of the rate of His antiport. The transport rate at 15 min was measured adding [$^3$H]His at the indicated concentration to proteoliposomes containing 10 mM internal His in the presence (●) or absence (○) of 100 mM Potassium gluconate. Data were plotted according to Michaelis - Menten equation. Results are mean ± S.D. from four independent experiments.

### 3.5. Oligomeric structure of hLAT1

The possible existence of a dimeric structure as predicted by bioinformatics (Fig. 1), was investigated. Fig. 9A shows Western Blot of recombinant hLAT1 analysed by electrophoresis under mild denaturing conditions on Sarkosyl-PAGE and stained by Anti-His. The presence of aggregates at higher molecular mass, in addition to the hLAT1 monomer, were observed. This indicated that the functional hLAT1 may have oligomeric composition. A similar analysis was performed on hLAT1 after insertion into proteoliposome membrane. In this case (Fig. 9A, lane 2), the oligomeric form of the protein was predominant. The apparent molecular mass of the monomeric and dimeric forms were lower than in lane 1; this was due to interference, during the run, of phospholipids deriving from proteoliposomes. To further analyze the presence of an oligomeric hLAT1 by SDS-PAGE, a cross-linking strategy was adopted. The solubilized protein was treated with $Cu^{++}$-phenanthroline which induces disulfide formation between vicinal Cys residues of proteins [45,46]. After treatment with the reagent, most of the protein migrated at a double molecular mass with respect to the untreated monomer (Fig. 9B, lane 2) due to formation of disulfide(s), confirming the existence of a prevalent dimeric form of hLAT1. To investigate the presence of oligomeric form of the protein in vivo, membranes from SiHa cells were solubilized and assayed with anti-LAT1 antibody (Fig. 9C). Solubilized sample was treated with DTE to separate CD98 from LAT1. Two major bands were observed under this condition, one at about 35 kDa and the other at about doubled molecular mass (Fig. 9C, lane 1). In the sample not treated with DTE (Fig. 9C, lane 2), a diffuse band was detected at an higher molecular mass

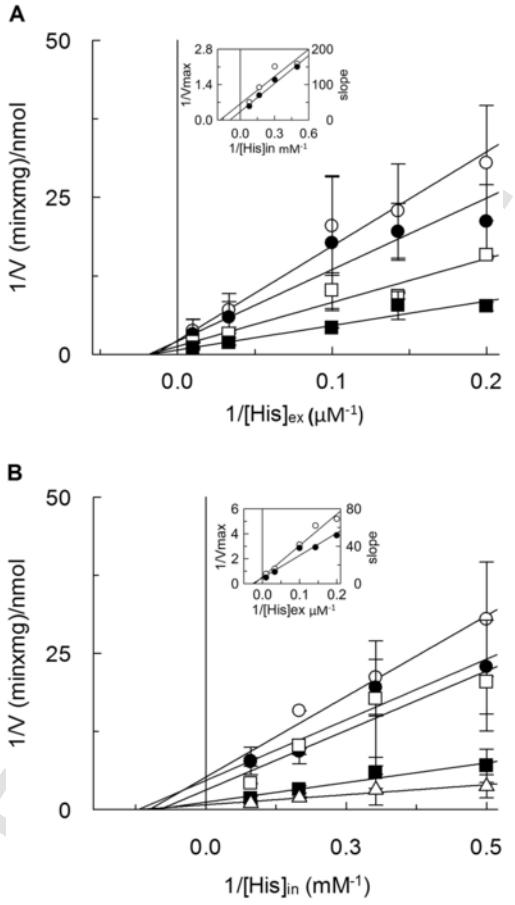


**Fig. 8.** Kinetics and Transport mechanism of the recombinant hLAT1. Data were analyzed by Lineweaver–Burk plots showing the dependence of reciprocal transport rate on reciprocal external (A) or internal (B) His concentrations. Transport reaction was stopped at 15 min as described in Section 2.5. In A), the concentrations of intraliposomal His were 2.0 (○), 3.3 (●), 6.0 (□), 12.5 (■) mM; the concentrations of external [$^3$H]His were 5.0, 7.0, 10, 33, 100 μM. In B) the same data of (A) were plotted as function of the internal His concentration at external [$^3$H]His 5.0 (○), 7.0 (●), 10 (□), 30 (■), 100 (Δ) μM. In A–B the insets show the re-plots of the intercepts on the Y-axis (1/Vmax - ○) or the slopes (Km/Vmax - ●) from the primary plots as a function of internal (A) or external (B) His. Results are mean ± S.D. from three independent experiments.

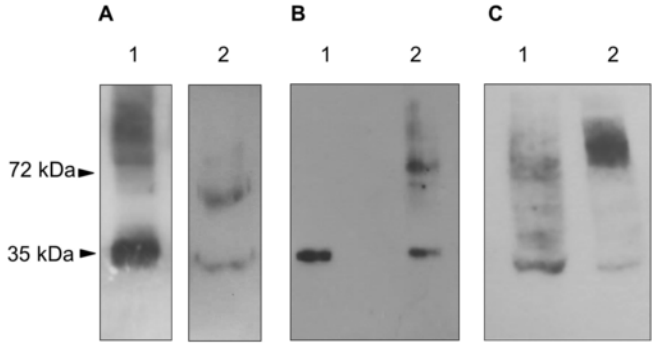


**Fig. 9.** Oligomeric state of recombinant and native hLAT1. In A) Purified and functional hLAT1 (lane 1) or hLAT1 inserted in proteoliposomes (lane 2) was subjected to electrophoresis under mild denaturing conditions, using sarkosyl (0.1%) instead of SDS (0.1%) in all run buffers without reducing agents in sample buffer. In B) purified and functional hLAT1 has been treated with 2 mM $Cu^{++}$-phenanthroline (lane 2) compared to untreated control (lane 1). After stopping cross-linking reaction, samples were run on a SDS-PAGE 10% without reducing agents in sample buffer. Protein monomers and oligomers were detected by immunoblotting analysis using anti-His antiserum 1:1000 dilution as described in Section 2.7 (A–B). In C) native hLAT1 was extracted from SiHa cell membrane and subjected to electrophoresis under mild denaturing conditions (as in 2A) treated (lane 1) or not (lane 2) with 100 mM DTE before running. Protein monomers and oligomers were detected by immunoblotting analysis using anti-LAT1 antiserum 1:2000 dilution as described in Section 2.7. Western blots (A–C) are representative of three independent experiments.

which may have an heterogeneous composition including hLAT1 homodimer and/or LAT1/CD98 heterodimer.

## 4. Discussion

In spite of the more than 450 papers dedicated to LAT1(CD98) (from Pubmed with "LAT1 (OR) SLC7A5" keyword entry in "Title & Abstract") of the last 10 years, no or only predictive information is available on the structure/function relationships of this important transporter. Therefore, we have invested efforts in advancing the molecular knowledge of transport mechanism. Two different crystallized structures, one of AdiC (e.g. PDB: 3L1L and the other of ApcT (e.g. PDB: 3GI9), can be used as distant homologous templates for hLAT1 comparative modelling. At the state of the art, the selection of the best template for modelling purposes is still challenging since the BLASTP and the HMM-based alignment are characterized by non-significantly different scores. We decided to base our modelling on the AdiC crystallographic structures, since more literature data supported this option [18,20,29]. Even though the homology model of LAT1 was built on the basis of AdiC, some relevant differences in term of molecular mechanism of substrate recognition are expected, since LAT1 accepts aromatic or aliphatic amino acids, while AdiC is mainly involved in interactions with the charged, Arg and Agmatine [2,29]. Indeed, W202 and W293 of AdiC are replaced in LAT1, respectively, by the more hydrophobic F252 according to Kyte-Doolittle [47] and by S342. These residues were previously predicted by bioinformatics to be involved in substrate recognition [18] but not experimentally proven, so far. In the present work, for the first time, the relationship of the F252 and S342 residues with substrate translocation has been demonstrated. In particular, F252 revealed to be essential as a gate of LAT1 as testified by disruptive effect of Ala substitution compared to F252W mutation and in analogy with structural data on AdiC [20]. However, the conservative substitution with W is not sufficient to restore proper affinity for substrate. An additional residue involved in substrate recognition and transport has been further identified, namely C335 which corresponds to C286 in AdiC (Figs. 1 and 3). This is mostly involved in substrate binding. Indeed, external Km increases up to 20 fold compared to WT. This result indicates that the thiol was the critical chemical group that is not present in Ala and that C335 represents a forefront residue for His binding. Another Cys residue was predicted to be part of the substrate binding site, namely C407. This residue, however, has a marginal role in substrate recognition since only the internal Km shows small variation upon mutation. The corresponding residue in AdiC is S357 (Figs. 1 and 3) whose side chain is more hydrophilic than that of Cys. Interestingly, AdiC in which this residue is mutated to Ala shows an affinity for substrate similar to that of WT as we observe in LAT1 [21]. Taken together, the results indicate: i) a switch from hydrophilic to neutral/hydrophobic substrate recognition between AdiC and LAT1; ii) that F252 is a gate element, allowing substrate entry in the translocation site playing, possibly, the same function as W202 in AdiC [20]; iii) that the other residues, i.e., S342 and C335 are responsible of substrate docking prior to translocation. Noteworthy, the prototype transporter with the same fold of LAT1, LeuT, shows critical residues more similar to LAT1 than AdiC, according to the more hydrophobic nature of LeuT substrates (not shown). This concept is also in agreement with predictions of a LAT1 wider binding site (smaller residues of the crucial amino acids) with respect to AdiC to accommodate larger amino acids [18].

C335A and C407A play a role in substrate handling and are not targeted by SH reagents either small, large, hydrophobic or hydrophilic, as shown by the unvaried sensitivity of C335A, C407A and C335/407A mutants to all these reagents. This means that the residues are not easily accessible by molecules other than substrates, i.e., the active site is accessible only upon substrate induced gating. Therefore, the high affinity of the transporter towards SH reacting compounds, mercurial or alkylating ones, is mediated by one or more of the other ten Cys residues. The mercury compounds do not interfere with the substrate path but impair conformational changes, according to the non-competitive inhibition caused by $HgCl_2$. Concerning the effect of $K^+$ and, at a similar extent, of $Na^+$ in stimulating the transport activity of LAT1 from the internal side, it might be due to a remnant cation binding site which is present in LeuT [48,49]. A similar effect by cations has been described for other membrane transporters of neutral amino acids, namely ASCT2, ASCT1 and B0AT1 which are stimulated/regulated by internal cations at physiological concentration [40,50,51]. Data on the kinetic mechanism of transport are in favor of a random simultaneous transport mechanism which implies formation of a ternary complex in which internal and external substrates are bound and translocated simultaneously towards opposed sides of the membrane. This type of mechanism cannot be easily explained by an alternating access model as that of LeuT [52,53] or APCS [54]. The simultaneous mechanism could however be explained by the existence of an oligomeric structure in which each single monomer can bind and translocate substrates from outside to inside or vice versa independently [40,41,55]. Data suggesting existence of hLAT1 dimeric structure are indeed in favor of the above described transport mechanism. Interestingly, AdiC, used as model and other similar eukaryotic transporters show also a dimeric organization [20,21,56–59]. Covalent dimer is observed upon treatment of the protein with S-S forming reagent; thus, it is likely that one (or more) Cys residue is located along the contact surface between the two monomers as highlighted by our model (Fig. 2) in which the residue C458 faces the homodimerization space, far from the C164 responsible of covalent interaction with CD98. Therefore, it can be hypothesized that also in cells hLAT1 can exist in a dimeric quaternary structure made by either homodimers of hLAT1 or dimers of the hLAT1/CD98 complex.

## 5. Conclusions

In this work, we improved the molecular knowledge on the human LAT1 transporter by using recombinant protein produced in *E. coli*, site-directed mutagenesis and transport assay in proteoliposomes. The residues F252, C335, S342 and C407 have been experimentally demonstrated to be critical for substrate binding and translocation shedding light on possible dimerization of the protein in cell membrane in analogy of APC transporters [20,21,56–59]. Since LAT1 is considered a valuable target for cancer therapy, the scenario resulting from these data represents also a step forward for studies aimed to identification of new potent and specific inhibitors that may have great outcome on human health.

## Transparency document

The Transparency document associated with this article can be found, in online version.

## Acknowledgments

This work was supported by grant from Italian MIUR, Ministero dell'Istruzione, dell'Università e della Ricerca [PON01_00937].

## Appendix A. Supplementary data

Supplementary data to this article can be found online at http://dx.doi.org/10.1016/j.bbagen.2017.01.013.

## References

[1] L. Mastroberardino, B. Spindler, R. Pfeiffer, P.J. Skelly, J. Loffing, C.B. Shoemaker, F. Verrey, Amino-acid transport by heterodimers of 4F2hc/CD98 and members of a permease family, Nature 395 (1998) 288–291.
[2] L. Napolitano, M. Scalise, M. Galluccio, L. Pochini, L.M. Albanese, C. Indiveri, LAT1 is the transport competent unit of the LAT1/CD98 heterodimeric amino acid transporter, Int. J. Biochem. Cell Biol. 67 (2015) 25–33.
[3] V. Ganapathy, M. Thangaraju, P.D. Prasad, Nutrient transporters in cancer: relevance to Warburg hypothesis and beyond, Pharmacol. Ther. 121 (2009) 29–40.
[4] L. Yang, T. Moss, L.S. Mangala, J. Marini, H. Zhao, S. Wahlig, G. Armaiz-Pena, D. Jiang, A. Achreja, J. Win, R. Roopaimoole, C. Rodriguez-Aguayo, I. Mercado-Uribe, G. Lopez-Berestein, J. Liu, T. Tsukamoto, A.K. Sood, P.T. Ram, D. Nagrath, Metabolic shifts toward glutamine regulate tumor growth, invasion and bioenergetics in ovarian cancer, Mol. Syst. Biol. 10 (2014) 728.
[5] C. Colas, P.M.U. Ung, A. Schlessinger, SLC transporters: structure, function, and drug discovery, Med. Chem. Commun. 7 (2016) 1069–1081.
[6] B.C. Fuchs, B.P. Bode, Amino acid transporters ASCT2 and LAT1 in cancer: partners in crime?, Semin. Cancer Biol. 15 (2005) 254–266.
[7] Y.D. Bhutia, E. Babu, S. Ramachandran, V. Ganapathy, Amino acid transporters in cancer and their relevance to "glutamine addiction": novel targets for the design of a new class of anticancer drugs, Cancer Res. 75 (2015) 1782–1788.
[8] Y. Zhao, L. Wang, J. Pan, The role of L-type amino acid transporter 1 in human tumors, Intractable Rare Dis. Res. 4 (2015) 165–169.
[9] Q. Wang, J. Holst, L-type amino acid transport and cancer: targeting the mTORC1 pathway to inhibit neoplasia, Am. J. Cancer Res. 5 (2015) 1281–1294.
[10] L. Pochini, M. Scalise, M. Galluccio, C. Indiveri, Membrane transporters for the special amino acid glutamine: structure/function relationships and relevance to human health, Front. Chem. 2 (2014) 61.
[11] M. Scalise, L. Pochini, M. Galluccio, C. Indiveri, Glutamine transport. From energy supply to sensing and beyond, Biochim. Biophys. Acta 1857 (2016) 1147–1157.
[12] R. Milkereit, A. Persaud, L. Vanoaica, A. Guetg, F. Verrey, D. Rotin, LAPTM4b recruits the LAT1-4F2hc Leu transporter to lysosomes and promotes mTORC1 activation, Nat. Commun. 6 (2015) 7250.
[13] M. Rebsamen, L. Pochini, T. Stasyk, M.E. de Araujo, M. Galluccio, R.K. Kandasamy, B. Snijder, A. Fauster, E.L. Rudashevskaya, M. Bruckner, S. Scorzoni, P.A. Filipek, K.V. Huber, J.W. Bigenzahn, L.X. Heinz, C. Kraft, K.L. Bennett, C. Indiveri, L.A. Huber, G. Superti-Furga, SLC38A9 is a component of the lysosomal amino acid sensing machinery that controls mTORC1, Nature 519 (2015) 477–481.
[14] S. Wang, Z.Y. Tsun, R.L. Wolfson, K. Shen, G.A. Wyant, M.E. Plovanich, E.D. Yuan, T.D. Jones, L. Chantranupong, W. Comb, T. Wang, L. Bar-Peled, R. Zoncu, C. Straub, C. Kim, J. Park, B.L. Sabatini, D.M. Sabatini, Metabolism. Lysosomal amino acid transporter SLC38A9 signals arginine sufficiency to mTORC1, Science 347 (2015) 188–194.
[15] J.M. Cantor, M.H. Ginsberg, CD98 at the crossroads of adaptive immunity and cancer, J. Cell Sci. 125 (2012) 1373–1382.
[16] L.R. de la Ballina, S. Cano-Crespo, E. Gonzalez-Munoz, S. Bial, S. Estrach, L. Cailleteau, F. Tissot, H. Daniel, A. Zorzano, M.H. Ginsberg, M. Palacin, C.C. Feral, Amino acid transport associated to cluster of differentiation 98 heavy chain (CD98hc) Is at the cross-road of oxidative stress and amino acid availability, J. Biol. Chem. 291 (2016) 9700–9711.
[17] E. Nakamura, M. Sato, H. Yang, F. Miyagawa, M. Harasaki, K. Tomita, S. Matsuoka, A. Noma, K. Iwai, N. Minato, 4F2 (CD98) heavy chain is associated covalently with an amino acid transporter and controls intracellular trafficking and membrane topology of 4F2 heterodimer, J. Biol. Chem. 274 (1999) 3009–3016.
[18] E.G. Geier, A. Schlessinger, H. Fan, J.E. Gable, J.J. Irwin, A. Sali, K.M. Giacomini, Structure-based ligand discovery for the large-neutral amino acid transporter 1, LAT-1, Proc. Natl. Acad. Sci. U. S. A. 110 (2013) 5480–5485.
[19] H. Ylikangas, K. Malmioja, L. Peura, M. Gynther, E.O. Nwachukwu, J. Leppanen, K. Laine, J. Rautio, M. Lahtela-Kakkonen, K.M. Huttunen, A. Poso, Quantitative insight into the design of compounds recognized by the L-type amino acid transporter 1 (LAT1), ChemMedChem 9 (2014) 2699–2707.
[20] X. Gao, L. Zhou, X. Jiao, F. Lu, C. Yan, X. Zeng, J. Wang, Y. Shi, Mechanism of substrate recognition and transport by an amino acid antiporter, Nature 463 (2010) 828–832.
[21] H. Ilgu, J.M. Jeckelmann, V. Gapsys, Z. Ucurum, B.L. de Groot, D. Fotiadis, Insights into the molecular basis for substrate binding and specificity of the wild-type L-arginine/agmatine antiporter AdiC, Proc. Natl. Acad. Sci. U. S. A. 113 (2016) 10358–10363.
[22] M. Galluccio, L. Pochini, V. Peta, M. Ianni, M. Scalise, C. Indiveri, Functional and molecular effects of mercury compounds on the human OCTN1 cation transporter: C50 and C136 are the targets for potent inhibition, Toxicol. Sci. 144 (2015) 105–113.
[23] S.N. Ho, H.D. Hunt, R.M. Horton, J.K. Pullen, L.R. Pease, Site-directed mutagenesis by overlap extension using the polymerase chain reaction, Gene 77 (1989) 51–59.
[24] M. Galluccio, P. Pingitore, M. Scalise, C. Indiveri, Cloning, large scale over-expression in E. coli and purification of the components of the human LAT 1 (SLC7A5) amino acid transporter, Protein J. 32 (2013) 442–448.
[25] L. Console, M. Scalise, Z. Tarmakova, I.R. Coe, C. Indiveri, N-linked glycosylation of human SLC1A5 (ASCT2) transporter is critical for trafficking to membrane, Biochim. Biophys. Acta 1853 (2015) 1636–1645.
[26] F. Palmieri, C. Indiveri, F. Bisaccia, V. Iacobazzi, Mitochondrial metabolite carrier proteins: purification, reconstitution, and transport studies, Methods Enzymol. 260 (1995) 349–369.
[27] E.M. Torchetti, C. Brizio, M. Colella, M. Galluccio, T.A. Giancaspero, C. Indiveri, M. Roberti, M. Barile, Mitochondrial localization of human FAD synthetase isoform 1, Mitochondrion 10 (2010) 263–273.
[28] L. Kowalczyk, M. Ratera, A. Paladino, P. Bartoccioni, E. Errasti-Murugarren, E. Valencia, G. Portella, S. Bial, A. Zorzano, I. Fita, M. Orozco, X. Carpena, J.L. Vazquez-Ibar, M. Palacin, Molecular basis of substrate-induced permeation by an amino acid antiporter, Proc. Natl. Acad. Sci. U. S. A. 108 (2011) 3935–3940.
[29] X. Gao, F. Lu, L. Zhou, S. Dang, L. Sun, X. Li, J. Wang, Y. Shi, Structure and mechanism of an amino acid antiporter, Science 324 (2009) 1565–1568.
[30] D. Van Der Spoel, E. Lindahl, B. Hess, G. Groenhof, A.E. Mark, H.J. Berendsen, GROMACS: fast, flexible, and free, J. Comput. Chem. 26 (2005) 1701–1718.
[31] Z. Guo, U. Mohanty, J. Noehre, T.K. Sawyer, W. Sherman, G. Krilov, Probing the alpha-helical structural stability of stapled p53 peptides: molecular dynamics simulations and analysis, Chem. Biol. Drug Des. 75 (2010) 348–359.
[32] H.J.C.P. Berendsen, J. P. M., W.F. van Gunsteren, A. DiNola, J.R. Haak, Molecular-dynamics with coupling to an external bath, J. Chem. Phys. 81 (1984) 3684–3690.
[33] S. Nosé, A unified formulation of the constant temperature molecular-dynamics methods, J. Chem. Phys. 81 (1984) 511–519.
[34] F. M., H. Eldesbrunner, R. Fu, J. Liang, Proceedings of the 28th Hawaii International Conference on Systems Science, 1995.
[35] Y. Fang, H. Jayaram, T. Shane, L. Kolmakova-Partensky, F. Wu, C. Williams, Y. Xiong, C. Miller, Structure of a prokaryotic virtual proton pump at 3.2 A resolution, Nature 460 (2009) 1040–1043.
[36] A. Krogh, B. Larsson, G. von Heijne, E.L. Sonnhammer, Predicting transmembrane protein topology with a hidden Markov model: application to complete genomes, J. Mol. Biol. 305 (2001) 567–580.
[37] R.J. Boado, J.Y. Li, C. Chu, F. Ogoshi, P. Wise, W.M. Pardridge, Site-directed mutagenesis of cysteine residues of large neutral amino acid transporter LAT1, Biochim. Biophys. Acta 1715 (2005) 104–110.

[38] Z. Yin, H. Jiang, T. Syversen, J.B. Rocha, M. Farina, M. Aschner, The methylmercury-L-cysteine conjugate is a substrate for the L-type large neutral amino acid transporter, J. Neurochem. 107 (2008) 1083–1090.
[39] C. Indiveri, A. Tonazzi, A. De Palma, F. Palmieri, Kinetic mechanism of antiports catalyzed by reconstituted ornithine/citrulline carrier from rat liver mitochondria, Biochim. Biophys. Acta 1503 (2001) 303–313.
[40] M. Scalise, L. Pochini, S. Panni, P. Pingitore, K. Hedfalk, C. Indiveri, Transport mechanism and regulatory properties of the human amino acid transporter ASCT2 (SLC1A5), Amino Acids 46 (2014) 2463–2475.
[41] C. Indiveri, L. Capobianco, R. Kramer, F. Palmieri, Kinetics of the reconstituted dicarboxylate carrier from rat liver mitochondria, Biochim. Biophys. Acta 977 (1989) 187–193.
[42] W.W. C., Stade state kinetics, In: The Enzymes, 2, 1970, pp. 1–65.
[43] O. Yanagida, Y. Kanai, A. Chairoungdua, D.K. Kim, H. Segawa, T. Nii, S.H. Cha, H. Matsuo, J. Fukushima, Y. Fukasawa, Y. Tani, Y. Taketani, H. Uchino, J.Y. Kim, J. Inatomi, I. Okayasu, K. Miyamoto, E. Takeda, T. Goya, H. Endou, Human L-type amino acid transporter 1 (LAT1): characterization of function and expression in tumor cell lines, Biochim. Biophys. Acta 1514 (2001) 291–302.
[44] Y. Kanai, H. Segawa, K. Miyamoto, H. Uchino, E. Takeda, H. Endou, Expression cloning and characterization of a transporter for large neutral amino acids activated by the heavy chain of 4F2 antigen (CD98), J. Biol. Chem. 273 (1998) 23629–23632.
[45] N. Reyes, C. Ginter, O. Boudker, Transport mechanism of a bacterial homologue of glutamate transporters, Nature 462 (2009) 880–885.
[46] I. Bartholomaus, L. Milan-Lobo, A. Nicke, S. Dutertre, H. Hastrup, A. Jha, U. Gether, H.H. Sitte, H. Betz, V. Eulenburg, Glycine transporter dimers: evidence for occurrence in the plasma membrane, J. Biol. Chem. 283 (2008) 10978–10991.
[47] J. Kyte, R.F. Doolittle, A simple method for displaying the hydropathic character of a protein, J. Mol. Biol. 157 (1982) 105–132.
[48] P.L. Shaffer, A. Goehring, A. Shankaranarayanan, E. Gouaux, Structure and mechanism of a $Na^+$-independent amino acid transporter, Science 325 (2009) 1010–1014.
[49] G. Khelashvili, S.G. Schmidt, L. Shi, J.A. Javitch, U. Gether, C.J. Loland, H. Weinstein, Conformational dynamics on the extracellular side of LeuT controlled by $Na^+$ and $K^+$ ions and the protonation state of Glu290, J. Biol. Chem. 291 (2016) 19786–19799.
[50] A.J. Scopelliti, G. Heinzelmann, S. Kuyucak, R.M. Ryan, R.J. Vandenberg, $Na^+$ interactions with the neutral amino acid transporter ASCT1, J. Biol. Chem. 289 (2014) 17468–17479.
[51] F. Oppedisano, C. Indiveri, Reconstitution into liposomes of the B degrees -like glutamine-neutral amino acid transporter from renal cell plasma membrane, Biochim. Biophys. Acta 1778 (2008) 2258–2265.
[52] D. Drew, O. Boudker, Shared molecular mechanisms of membrane transporters, Annu. Rev. Biochem. 85 (2016) 543–572.
[53] G. Rudnick, R. Kramer, R.D. Blakely, D.L. Murphy, F. Verrey, The SLC6 transporters: perspectives on structure, functions, regulation, and models for transporter dysfunction, Pflugers Arch. 466 (2014) 25–42.
[54] L.R. Forrest, R. Kramer, C. Ziegler, The structural basis of secondary active transport mechanisms, Biochim. Biophys. Acta 1807 (2011) 167–188.
[55] K. Khafizov, R. Staritzbichler, M. Stamm, L.R. Forrest, A study of the evolution of inverted-topology repeats from LeuT-fold transporters using AlignMe, Biochemistry 49 (2010) 10702–10713.
[56] F. Casagrande, M. Ratera, A.D. Schenk, M. Chami, E. Valencia, J.M. Lopez, D. Torrents, A. Engel, M. Palacin, D. Fotiadis, Projection structure of a member of the amino acid/polyamine/organocation transporter superfamily, J. Biol. Chem. 283 (2008) 33240–33248.
[57] Y. Fang, L. Kolmakova-Partensky, C. Miller, A bacterial arginine-agmatine exchange transporter involved in extreme acid resistance, J. Biol. Chem. 282 (2007) 176–182.
[58] Y. Alguel, S. Amillis, J. Leung, G. Lambrinidis, S. Capaldi, N.J. Scull, G. Craven, S. Iwata, A. Armstrong, E. Mikros, G. Diallinas, A.D. Cameron, B. Byrne, Structure of eukaryotic purine/H(+) symporter UapA suggests a role for homodimerization in transport activity, Nat. Commun. 7 (2016) 11336.
[59] G. Diallinas, Dissection of transporter function: from genetics to structure, Trends Genet. 32 (2016) 576–590.